THE JOURNAL OF PHYSICAL CHEMISTRY C

Article

Cite This: J. Phys. Chem. C 2019, 123, 16300−16307

pubs.acs.org/JPCC

Spontaneous Formation of Tetrahydrofuran Hydrate in Ultrahigh Vacuum

Jyotirmoy Ghosh, Radha Gobinda Bhuin,[†] Gopi Ragupathy,[‡] and Thalappil Pradeep*

DST Unit of Nanoscience (DST UNS) and Thematic Unit of Excellence (TUE), Department of Chemistry, Indian Institute of Technology Madras, Chennai 600036, India

Supporting Information

ABSTRACT: Clathrate hydrates (CHs) typically nucleate under high-pressure conditions, but their existence in ultrahigh vacuum (UHV) is an open question. Here, we report the formation of tetrahydrofuran (THF) hydrate in UHV, using reflection absorption infrared spectroscopy (RAIRS). Annealing both sequentially and co-deposited mixtures of THF and H_2O to 130 K for adequate time, originally prepared at 10 K, led to the formation of THF hydrate, at 10^{-10} mbar. Nucleation of THF hydrate was associated with the crystallization of amorphous solid water. Crystallization kinetics was examined through isothermal kinetic measurements using RAIRS in the temperature range of 120−130 K. The kinetic measurements revealed that the THF hydrate formation was a diffusion-controlled process and the overall activation energy for the process was found to be ~23.12 kJ mol^{-1}. This considerably lower activation energy as compared to that for the crystallization of pure ice established the spontaneity of the process. The results provide valuable insights into the low-pressure characteristics of CHs and associated thermodynamics.

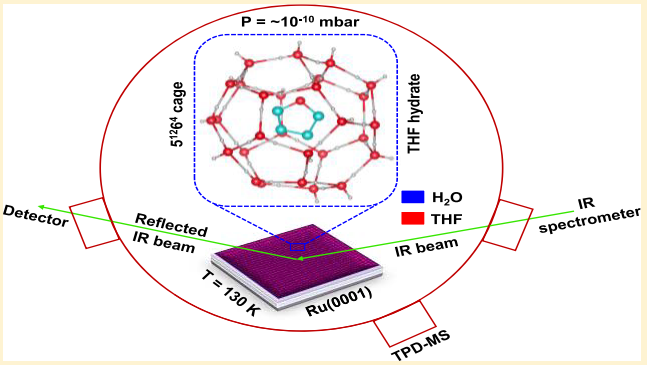

INTRODUCTION

Clathrate hydrates (CHs) are solid inclusion compounds, which are crystalline and contain guest molecules in the hydrogen-bonded water cages.[1−3] There are several guest molecules such as CH_4, CO_2, tetrahydrofuran (THF), etc., which could potentially form CHs at different conditions. These hydrates are found in ocean floor and permafrost regions of the earth.[1] CHs are important materials in terms of their wide applications in the areas of H_2 storage,[4−7] renewable energy,[8] CO_2 sequestrations,[9] and desalination.[10] High pressure and ambient[11] or low temperature[12] are the essential conditions for the formation of CHs. However, the requirement of high pressures for the nucleation of CHs is disadvantageous from an application point of view. Our present study reveals that such compounds are indeed feasible to form at extreme conditions. We have recently shown that methane and CO_2 can form hydrates at 10^{-10} mbar and 10−30 K, conditions analogous to space.[13] The presence of CHs in space was speculated for long.[3,14] Interaction of the trapped species with vapor-deposited amorphous solid water (ASW) plays important roles in the formation of CHs. This implies the feasibility of CH formation over a wide temperature and pressure window.

ASW has significant relevance to chemical,[15,16] biological,[17] physical,[18] astrophysical,[19,20] and materials sciences.[21,22] It is highly porous and formed by vapor deposition at temperatures below 120 K. Its porous morphology facilitates the entrapment of different species within the ASW network.[20,23] Interaction of the entrapped species with ASW can lead to different phenomena like phase segregation,[24] homogeneous mixing,[25] diffusion,[26] H-bonding,[27] chemical reaction,[28] CH formation,[13,29−31] etc. Among different known CHs, THF hydrate has drawn special interest as it can recover CO_2 from flue gas[32] as well as store hydrogen.[5,6,33] In general, THF forms the s-II hydrate structure below T = 277.6 K and at 5 kPa (50 mbar).[34,35] According to the calculation of dissociation pressures of different hydrates,[3] it should be stable at low pressures and low temperatures. In view of the possible formation of CHs under vacuum or low pressure, various methods were developed to observe this process, such as direct vapor deposition,[12] annealing an appropriate solid mixture to the required temperature,[31] and interaction of the guest molecule in the vapor phase with ice nanocrystals.[36,37] Richardson et al. showed that THF hydrate can be formed under vacuum (~1 μ or ~1.33 × 10^{-3} mbar) by vapor deposition.[31] Hallbrucker and co-workers have shown the formation of CHs of NO,[38] N_2,[39−41] O_2,[39−43] CO,[40] and Ar[40] from vapor-deposited ASW in a high vacuum (~10^{-6} mbar) experimental chamber, which was subsequently pressurized with 1 bar "external" pressure of the guest molecule. Here, we

Received: May 8, 2019
Revised: June 12, 2019
Published: June 13, 2019

DOI: 10.1021/acs.jpcc.9b04370
J. Phys. Chem. C 2019, 123, 16300−16307

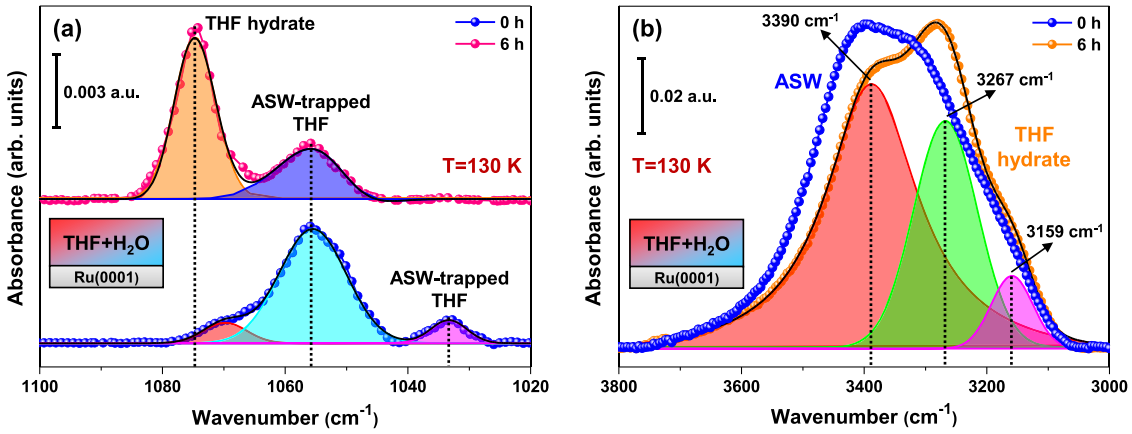

Figure 1. Isothermal time-dependent RAIR spectra of 300 MLs of a THF/H_2O (1:5) mixture (a) in the asymmetric C−O stretching region and (b) in the O−H stretching region, at 130 K. Prior to data collection, the mixture was co-deposited on the Ru(0001) substrate at 10 K and annealed at a rate of 2 K min^{-1} to 130 K. In (b), the spectrum labeled 6 h was deconvoluted to show its components and the spectrum of ASW was multiplied by 1.5 to match the intensity with the former.

have studied the formation of THF hydrate at ~10^{-10} mbar and 120−130 K by surface-sensitive reflection absorption infrared spectroscopy (RAIRS). We have also studied the associated kinetics and explored the thermodynamic parameters. THF is known to be a stabilizing guest or promoter for the formation of binary CHs.[33,44] So far, there are no experimental studies to the best of our knowledge on the formation of THF hydrate at extremely low pressures like ~10^{-10} mbar. This study can help in further exploring the formation and stabilization of binary CHs in ultrahigh vacuum (UHV).

In the experiments, we co-deposited a 1:5 mixture of THF and water from their vapor phase to a precooled Ru(0001) substrate at 10 K inside a UHV chamber.[45] Annealing the mixture to 130 K and keeping it for 6 h led to the formation of THF hydrate. RAIRS was used to monitor hydrate formation. Evolution of THF hydrate showed temperature-dependent kinetics, which was established by carrying out a time-dependent RAIRS study of similar systems at different temperatures. The time-dependent RAIRS study at 130 K also showed the formation of THF hydrate in the case of sequential deposition (THF@H_2O).

EXPERIMENTAL SECTION

The experiments were conducted in a UHV chamber with a base pressure of ~5 × 10^{-10} mbar. The UHV chamber has been described in detail elsewhere.[45] Briefly, the chamber was equipped with RAIRS and temperature-programmed desorption mass spectrometry facilities. The substrate, a Ru(0001) single crystal, was cooled by a closed-cycle helium cryostat to 10 K. The substrate temperature was measured using a K-type thermocouple wire connected to it. The substrate was cleaned by heating to 400 K multiple times prior to vapor deposition. Desired molecular solid films were grown on Ru(0001) by vapor deposition at 10 K. The surface coverage of molecular solids was represented in terms of monolayers (MLs)[46] assuming that 1.33 × 10^{-6} mbar s = 1 ML, which was estimated to contain ~1.1 × 10^{15} molecules cm^{-2}. In a number of earlier reports,[47,48] such calculation was used for the estimation of surface coverages. One point to be noted is that all of the experiments were performed under multilayer deposition conditions; therefore, the substrate does not play any role in the processes mentioned here.

THF (Sigma-Aldrich, 99%) and H_2O (Milli-Q, 18.2 MΩ resistivity) were purified by multiple freeze−pump−thaw cycles. The molecular solids of water and THF were prepared on a Ru(0001) substrate by sequential and co-deposition methods as per the need of the experiment. The vapors of THF and water were backfilled into the UHV chamber through variable all-metal leak valves. For the deposition of 300 MLs of (1:5) mixed THF and water, the chamber was backfilled at a total pressure of ~5 × 10^{-7} mbar (where THF and water partial pressures were 1 × 10^{-7} and 4 × 10^{-7} mbar, respectively, monitored by the mass spectrometer during deposition) and the mixture was exposed to the substrate for 10 min. To prepare other mixtures, the partial pressures of the individual components were set as per their requirement. The deposited mixed ice was slowly annealed (heating rate = 2 K min^{-1}) to 130 K, and time-dependent RAIR spectra were recorded. RAIRS measurements were performed using a Bruker FT-IR spectrometer, Vertex 70 with a liquid-nitrogen-cooled mercury cadmium telluride detector. The IR beam path outside the UHV chamber was purged with dry nitrogen gas. All RAIR spectra were collected in the 4000−550 cm^{-1} range with 2 cm^{-1} spectral resolution, averaged over 512 scans.

Computational Details. The three most common cages of CHs were considered for calculations. Geometry optimizations for the water cages and the host−guest complexes were performed using the B3LYP method in conjunction with the 6-311++G(d,p) basis set. All of the optimized geometries in this work were confirmed to be minima in the potential energy surface by the absence of imaginary frequencies in vibrational frequency analysis. It was shown that this basis set produced quite well all of the geometries, frequencies, and electric properties of THF hydrate.[49] The electronic structure calculations were performed using the GAUSSIAN 09 program.[50] The input configurations of the water cages were taken from our previous work and were subsequently optimized.[13] The optimized structures corresponding to the 5^{12}, $5^{12}6^2$, and $5^{12}6^4$ cages are shown later. It was observed that the $5^{12}6^4$ THF hydrate cage was quite stable; stability also depends on the size of the guest molecule.

RESULTS AND DISCUSSION

Figure 1a shows the RAIR spectra of 300 MLs of a THF/H_2O mixture (1:5), which was co-deposited at 10 K on the

DOI: 10.1021/acs.jpcc.9b04370
J. Phys. Chem. C 2019, 123, 16300−16307

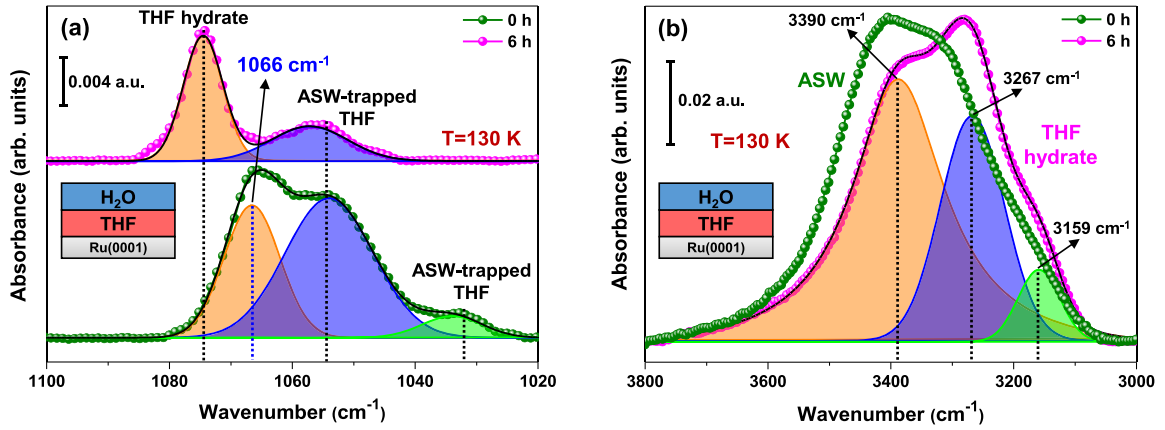

Figure 2. Time-dependent RAIR spectra of 300 MLs of a THF@H_2O mixture (1:1) in the (a) asymmetric C−O stretching region and (b) O−H stretching region, which was sequentially deposited at 10 K on the Ru(0001) substrate. This mixture was annealed at a rate of 2 K min^{-1} to 130 K. In (b), the spectrum labeled 6 h was deconvoluted to show its components and the spectrum of ASW was multiplied by 1.5 to match the intensity with the former.

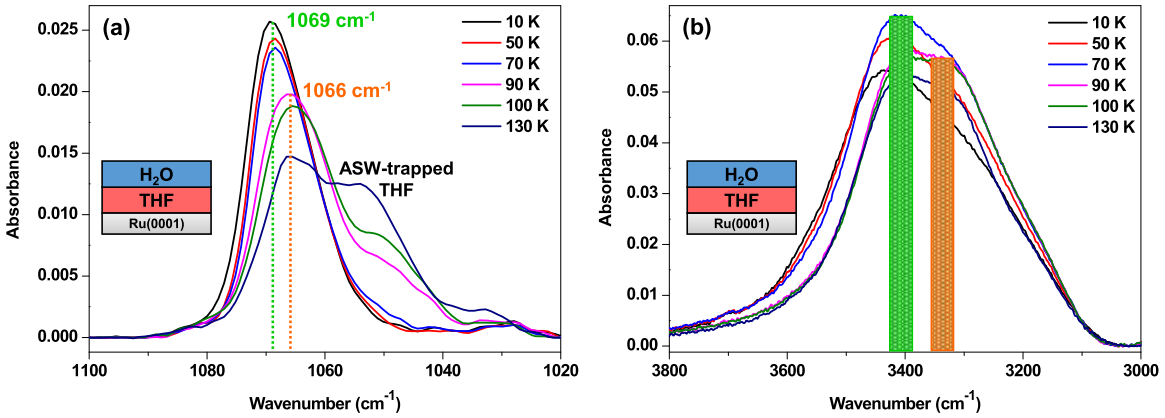

Figure 3. Temperature-dependent RAIR spectra of 300 MLs of a THF@H_2O mixture (1:1) in the (a) asymmetric C−O stretching region and (b) O−H stretching region, which was sequentially deposited at 10 K on the Ru(0001) substrate. The sequential deposition was carried by condensing 150 MLs of H_2O film over the same coverage of THF film, thus making it a (1:1) mixture. This mixture was annealed at 2 K min^{-1} heating rate, and the spectra were collected.

Ru(0001) substrate. After deposition, it was slowly heated at 2 K min^{-1} to 130 K and kept at this temperature for 6 h. Water is known to have orientational freedom at this temperature.[51] Due to such motions, molecular organization can occur in the process of annealing. We note that isothermal annealing for extended periods on the order of the tens of hours was essential to form hydrates of methane at cryogenic conditions.[13] The RAIR spectrum was measured immediately after heating to 130 K, which represents the 0 h spectrum. Here, the asymmetric C−O stretching band of THF showed two peaks at ∼1034 and ∼1053 cm^{-1}, which were due to THF trapped in different sites of ASW.[31] The shoulder at 1070 cm^{-1} converted gradually to a new peak at ∼1074 cm^{-1} after 6 h at 130 K (time-dependent spectra for each time interval are presented in Figure S1). This new peak is the characteristic feature of the asymmetric C−O stretching of THF hydrate.[27,30,49,52] It serves as a convenient indicator of THF hydrate since it lies well above the IR peak positions of other likely condensed phases of THF.[30,31,36] The intensity of this new peak continued to increase over time, while the intensity of other two peaks reduced gradually. After 6 h, the intensity of this new peak reached a maximum, whereas that of the 1034 cm^{-1} peak was reduced almost to zero. This suggests the conversion of THF hydrate from the ASW-trapped THF.

Figure 1b depicts the corresponding data in the O−H stretching region. The broad peak present originally got ordered and red-shifted with time, which is an indication of crystallization.[53−55] Therefore, it can be concluded that THF gradually transformed into its hydrate structure at 130 K over 6 h; consequently, the morphology of the ice film turns to crystalline from its amorphous phase. The O−H stretching band for the THF hydrate was deconvoluted to show its components. To eliminate the possibility of self-crystallization of ice, we have shown in Figure S2a,b that ice by itself is not capable of forming its crystalline analogue over time at 120 and 130 K. It needs a higher temperature (∼145 K; crystallization temperature of ice) in the absence of a guest molecule.[51]

We further investigated whether co-deposition was a prerequisite for hydrate formation. To check this, 150 MLs of THF were first deposited on Ru(0001) at 10 K, and subsequently, the film was covered with 150 MLs of H_2O. This sequential deposition is represented as THF@H_2O. It was annealed at 2 K min^{-1} to 130 K, and time-dependent spectra were collected as shown in Figure 2. The asymmetric C−O stretching region in Figure 2a shows IR features at 1066, 1053, and 1034 cm^{-1} at 0 h at 130 K. These two peaks at ∼1034 and ∼1053 cm^{-1} are due to THF trapped in different sites of ASW, as explained earlier. The origin of the ∼1066 cm^{-1} peak can be

DOI: 10.1021/acs.jpcc.9b04370
J. Phys. Chem. C 2019, 123, 16300−16307

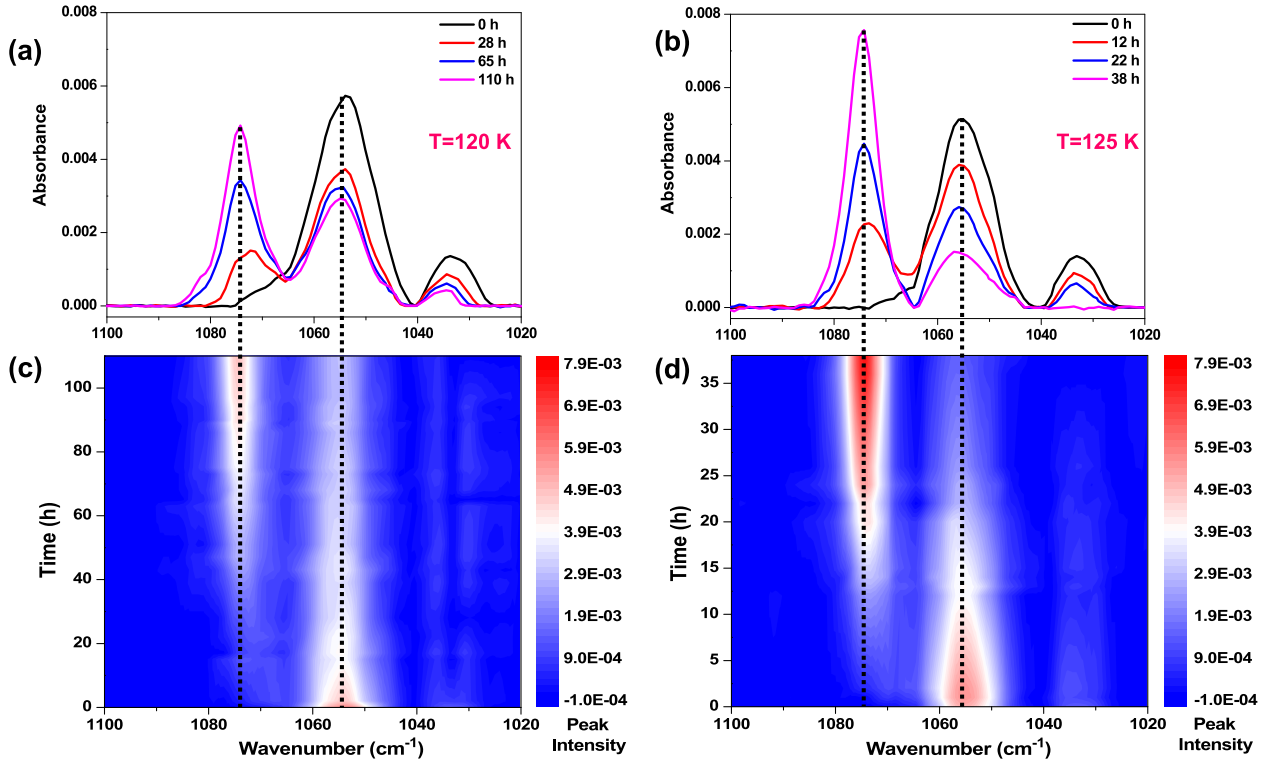

Figure 4. Time-dependent RAIR spectra of 300 MLs of a THF/H_2O mixture (1:5) at (a) 120 K and (b) 125 K, in the asymmetric C−O stretching region; the mixture was co-deposited at 10 K on the Ru(0001) substrate. This mixture was annealed at 2 K min^{-1} to the respective temperatures. Variation of the IR peak intensities of 1053 and 1074 cm^{-1}, plotted as a contour plot as a function of time at (c) 120 K and (d) 125 K. Intensity values are on the right.

explained from temperature-dependent RAIR spectra of a THF@H_2O mixture (Figure 3a), where the same peak was observed at 90 K and beyond. The peak at ∼1066 cm^{-1} is due to the formation of irregular THF crystallites. These crystallites form due to the diffusion of THF into the over layers of the ASW network, at ≥90 K. Pure THF undergoes crystallization at >90 K, as observed from an independent study composed of 150 MLs (Figure S3). As shown in Figure 3b, at 90 K, the O−H stretching band shifts to a lower wavenumber, as indicated by the vertical bars of two different colors (green and orange). This again supports the formation of irregular THF crystallites within the ASW pores, which influences the ASW network. This type of diffusion of dichloromethane followed by crystallization has been reported previously.[56]

Interestingly, the sequential deposition does not lead to the formation of THF hydrate just by annealing, as the characteristic peak (∼1074 cm^{-1}) of the same was not observed in Figure 3a. However, the formation of THF hydrate was observed only when this THF@H_2O film was kept at 130 K for a few hours (time-dependent spectra for each time interval are presented in Figure S4). The characteristic THF hydrate peak at ∼1074 cm^{-1} started appearing with time and becomes more prominent after 6 h as shown in Figure S4. Alongside, the broad O−H stretching band also attained crystalline features with time. Diffusion of THF into the overlayer ice network took place by annealing as explained before. After diffusion, a fraction of THF molecules got trapped as the ASW pores collapsed by annealing. Several studies suggest that ASW possesses a porous structure and the porosity disappears upon annealing.[57−59] After the diffusion and the collapse of ASW pores by annealing, THF molecules got sufficient time to interact with the water molecules, which resulted in the THF hydrate. It can be concluded from here that both sequential and co-deposition methods can result in THF hydrate provided sufficient time for intermolecular interaction between THF and water. Diffusion plays a significant role in facilitating the interaction.

We examined the effect of temperature on the formation of THF hydrate. Figure 4a,b shows the time-dependent RAIR spectra of a 1:5 THF/H_2O mixture in the asymmetric C−O stretching region of THF at 120 and 125 K, respectively. In contour plots (Figure 4c,d), the intensities of peaks at 1053 and 1074 cm^{-1} are plotted to follow the hydrate formation. At 120 K, the rate of conversion of THF hydrate is so slow that even after 110 h it is incomplete (Figure 4a).

However, at 125 K, the rate of conversion is relatively faster as the 1074 cm^{-1} peak showed substantial intensity within 38 h. Earlier, we observed that it required not less than 6 h at 130 K for substantial nucleation of THF hydrate. This demonstrates that the formation of THF hydrate is a temperature- and time-dependent process, and it follows certain kinetics.

It was observed that the formation of THF hydrate was associated with the crystallization of ASW (Figures 1b and 2b) and that the crystallization process showed both time- and temperature-dependent kinetics. The progress of crystallization was followed monitoring the evolution of the 1074 cm^{-1} peak. Here, the intensity of the 1074 cm^{-1} peak is proportional to the extent of clathrate formation, which in turn is a measure of crystallization of the ice. We have observed that with the enhancement of this peak intensity, the O−H stretching became more ordered, indicating crystallinity of the ice as shown in Figure S1. We have followed the crystallization kinetics by isothermal annealing experiments conducted at different temperatures. Here, we used the Avrami equation that

DOI: 10.1021/acs.jpcc.9b04370
J. Phys. Chem. C 2019, 123, 16300−16307

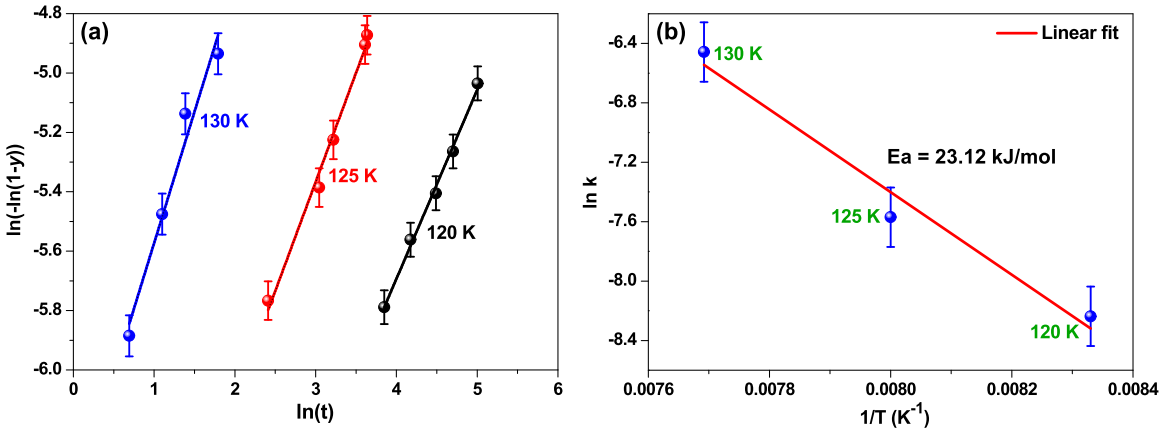

Figure 5. (a) Plot of $\ln(-\ln[1 - y(T)])$ vs $\ln(t)$ at different temperatures of 130, 125, and 120 K. The data points were fitted using the Avrami equation (eq 2). These data correspond to a straight line. (b) Plot of $\ln k(T)$ vs inverse temperature $(1/T)$. The data points were fitted to obtain a straight line. Activation energy (E_a) can be calculated from the slope of the straight line.

describes the extent of crystallization (y) as a function of time (t) during isothermal annealing at temperature T.[60−62] The equation is as follows

$$y(T) = 1 - \exp[-k(T)\cdot t^n] \quad (1)$$

where t is the time, $k(T)$ is the rate constant, and n is related to the crystallization mechanism. For all temperatures, n is a parameter whose magnitude is determined by the geometry of the growing particles and whether the transformation is diffusion- or interface-controlled.[60,62] For an interface-controlled transformation, n is an integer from 1 to 4, depending upon the shape of the particle, whereas in a diffusion-controlled transformation, n is usually a fraction except for the cylindrical geometry of the particle when it is equal to 1.[62,63] Thus, the nature of crystallization process can be predicted from the knowledge of the parameter n. To find out the values of n and $k(T)$ at different temperatures, eq 1 can be rewritten as

$$\ln(-\ln[1 - y(T)]) = n \ln(t) + \ln k(T) \quad (2)$$

Figure 5a shows three linearly fitted straight lines corresponding to three different temperatures. These data points were obtained using eq 2, where the extent of crystallization (y) was assumed to be directly proportional to the intensity of the 1074 cm^{-1} peak (THF hydrate), as explained before. The slope of each straight line corresponds to the value of n at different temperatures. The rate constants of the crystallization process, which in turn is the formation of hydrate at different temperatures, can be evaluated from the intercept values (from eq 2) of each straight line (Figure 5a). Once the rate constant is known at different temperatures, it is possible to calculate the activation energy involved in the process. The values of n and the rate constants at different temperatures are given in Table 1. Here, the fractional values of n indicate that the crystallization process or the formation of CH is diffusion-controlled, as mentioned earlier. It is already known, according to the criteria for the values of n, that the crystallization kinetics of water at $T < 150$ K is diffusion-controlled.[62]

Table 1. Parameters for Crystallization of Water During the Formation of THF Hydrate at Different Temperatures

temperature (K)	n	rate constant; k (s^{-1})
120	0.64	2.64×10^{-4}
125	0.73	5.16×10^{-4}
130	0.88	1.57×10^{-3}

The experimental data as shown in Figure 5b were fitted to the Arrhenius equation. The slope of this line gives the activation energy (E_a), which was estimated to be ~23.12 kJ mol^{-1}. This is lesser than the previously reported activation energy (E_a) values (60−77 kJ mol^{-1}) for crystallization of pure ASW obtained by different experimental techniques.[64−68] This considerably lower activation energy suggests the feasibility of the process; however, the process is kinetically hindered at such low temperature due to limited diffusion. At elevated temperature, due to thermal motion of the molecules, the entropy of the system is increased, which in turn enhances the diffusion process and results in hydrate formation. At a temperature of 120 K or above, H_2O ice undergoes a structural change,[51] and this temperature is very close to the desorption temperature of THF; therefore, these molecules also possess sufficient thermal motion. A combination of these two effects may be responsible for the formation of the hydrate. Due to hydrate formation, the system reaches a thermodynamically stable crystalline structure.

It would be interesting to know about the structures of THF hydrates that are formed at such low pressures. One would expect that the low-pressure hydrate can be structurally different from the conventional high-pressure hydrates. Unfortunately, our experimental setup is not equipped with in situ diffraction tools, neither it has a setup to transfer the sample for diffraction studies to get insight into the structural details. We have compared the O−H stretching of THF hydrate, cubic ice (I_c), and hexagonal ice (I_h) as shown in Figure S5. The crystalline forms (hexagonal and cubic) of ice were prepared separately by annealing 150 MLs of ASW to respective crystallization temperatures. It was observed that the O−H stretching of THF hydrate is similar in shape to hexagonal ice than that of cubic ice (Figure S5). We may conclude that during the formation of THF hydrate the overall ice is attaining a structure comparable to the hexagonal ice. We note that THF hydrate is known to form s-II hydrate, which is cubic in nature. Computationally, optimized structures of THF entrapped in different CH cages (5^{12}, $5^{12}6^2$, and $5^{12}6^4$) are shown in Figure 6. These calculated structures revealed that a large cage ($5^{12}6^4$) is favored for the entrapment of THF, whereas the other two cages are unstable. Formation of THF

DOI: 10.1021/acs.jpcc.9b04370
J. Phys. Chem. C 2019, 123, 16300−16307

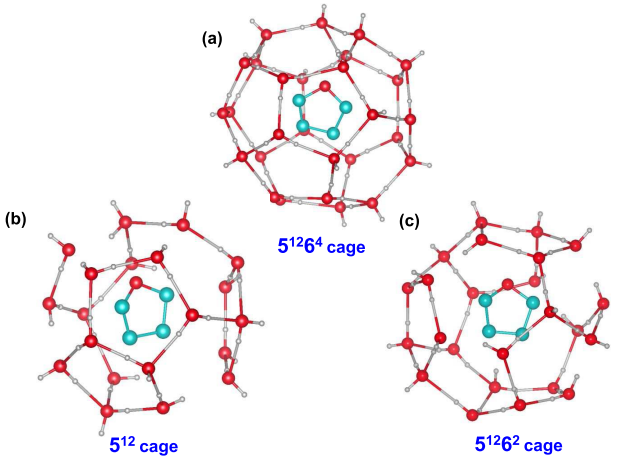

Figure 6. DFT-optimized structures of THF trapped within different CH cages, such as (a) $5^{12}6^4$ cage, (b) 5^{12} cage, and (c) $5^{12}6^2$ cage. Here, water cage and the guest molecule (THF) are shown. H atoms of THF molecules in all of the structures are omitted for clarity. Color code used: cyan, C; red, O; and gray, H.

hydrate around atmospheric pressure reveals that due to the large size of the THF molecule, it forms an s-II hydrate structure and occupies the large cage ($5^{12}6^4$).[34] Here, the computed shift in the C−O asymmetric mode of the $5^{12}6^4$ cage closely matches the experimental shift of the same (Table S1). Other possible cages computed ($5^{12}6$ and $5^{12}6^2$) have a reduced or an opposite shift, respectively (Table S1). In Table S2, we have presented the coordinates of the optimized geometries of THF in 5^{12}, $5^{12}6^2$, and $5^{12}6^4$ CH cages.

In this paper, we have discussed a suitable method to form spontaneous and stable THF hydrate at cryogenic conditions under UHV. The hydrate formation is found to be diffusion-controlled and is associated with the formation of the thermodynamically stable crystalline structure at a lower than usual crystallization temperature of ice. Kinetic measurements reveal that the crystallization process at <120 K is kinetically hindered due to limited motion of the guest and host molecules. However, upon achieving significant molecular motion or mobility at a warmer temperature (near 130 K or above), both THF and water molecules rearrange themselves to form the more stable hydrate structure.

CONCLUSIONS

In conclusion, we have studied the formation of THF hydrate at cryogenic temperatures in UHV using surface-sensitive RAIRS. THF hydrate forms in the temperature range of 120−130 K and at 10^{-10} mbar. We find that co-deposition as well as sequential deposition of THF and H_2O results in the formation of THF hydrate. IR spectral analysis of the O−H stretching region suggests that the hydrate formation is associated with the conversion of ASW to its crystalline analogue. This conversion follows both time- and temperature-dependent kinetics, and we calculated the activation energy (E_a) for this process. Kinetic studies showed reduced overall activation energy, which makes the formation of THF hydrate spontaneous even in UHV. This approach provides an opportunity to explore the formation of CHs in extreme or ultralow (P, T) regions of the phase diagram that were previously inaccessible due to experimental limitations. In addition, there is a future scope to study certain binary CHs in UHV, since THF hydrate acts as a stabilizer or promoter for their formation.

ASSOCIATED CONTENT

Supporting Information

The Supporting Information is available free of charge on the ACS Publications website at DOI: 10.1021/acs.jpcc.9b04370.

Time- and temperature-dependent IR spectra; comparison of the experimental and computational vibrational shifts; Cartesian coordinates of the hydrates; and comparison of IR spectra of THF hydrate, cubic ice, and hexagonal ice (PDF)

AUTHOR INFORMATION

Corresponding Author

*E-mail: pradeep@iitm.ac.in.

ORCID

Thalappil Pradeep: 0000-0003-3174-534X

Present Addresses

†Lehrstuhl für Physikalische Chemie II, Friedrich-Alexander-Universität Erlangen-Nürnberg, Egerlandstr. 3, 91058 Erlangen, Germany (R.G.B.).

‡The Institute of Chemistry and The Farkas Center for Light-Induced Processes, The Hebrew University of Jerusalem, Givat Ram, Jerusalem 91904, Israel (G.R.).

Author Contributions

J.G. designed and performed the experiments. J.G., R.G.B., and G.R. analyzed the results. G.R. carried out the calculations. T.P. proposed the project and supervised the progress. The manuscript was written through contributions of all authors.

Notes

The authors declare no competing financial interest.

ACKNOWLEDGMENTS

J.G. thanks the University Grants Commission (UGC) for his research fellowship. We thank the Department of Science and Technology (DST), Government of India, for supporting our research.

REFERENCES

(1) Sloan, E. D., Jr. Fundamental principles and applications of natural gas hydrates. *Nature* **2003**, *426*, 353−363.

(2) Ripmeester, J. A.; Tse, J. S.; Ratcliffe, C. I.; Powell, B. M. A new clathrate hydrate structure. *Nature* **1987**, *325*, 135−136.

(3) Miller, S. L. The occurrence of gas hydrates in the solar system. *Proc. Natl. Acad. Sci. U.S.A.* **1961**, *47*, 1798−1808.

(4) Mao, W. L.; Mao, H.-k.; Goncharov, A. F.; Struzhkin, V. V.; Guo, Q.; Hu, J.; Shu, J.; Hemley, R. J.; Somayazulu, M.; Zhao, Y. Hydrogen Clusters in Clathrate Hydrate. *Science* **2002**, *297*, 2247−2249.

(5) Sugahara, T.; Haag, J. C.; Prasad, P. S. R.; Warntjes, A. A.; Sloan, E. D.; Sum, A. K.; Koh, C. A. Increasing Hydrogen Storage Capacity Using Tetrahydrofuran. *J. Am. Chem. Soc.* **2009**, *131*, 14616−14617.

(6) Lee, H.; Lee, J.-w.; Kim, D. Y.; Park, J.; Seo, Y.-T.; Zeng, H.; Moudrakovski, I. L.; Ratcliffe, C. I.; Ripmeester, J. A. Tuning clathrate hydrates for hydrogen storage. *Nature* **2005**, *434*, 743−746.

(7) Mao, W. L.; Mao, H.-k. Hydrogen storage in molecular compounds. *Proc. Natl. Acad. Sci. U.S.A.* **2004**, *101*, 708−710.

(8) Khurana, M.; Yin, Z.; Linga, P. A Review of Clathrate Hydrate Nucleation. *ACS Sustainable Chem. Eng.* **2017**, *5*, 11176−11203.

(9) Park, Y.; Kim, D.-Y.; Lee, J.-W.; Huh, D.-G.; Park, K.-P.; Lee, J.; Lee, H. Sequestering carbon dioxide into complex structures of naturally occurring gas hydrates. *Proc. Natl. Acad. Sci. U.S.A.* **2006**, *103*, 12690−12694.

(10) Kang, K. C.; Linga, P.; Park, K.-n.; Choi, S.-J.; Lee, J. D. Seawater desalination by gas hydrate process and removal characteristics of dissolved ions (Na^+, K^+, Mg^{2+}, Ca^{2+}, B^{3+}, Cl^-, SO_4^{2-}). *Desalination* **2014**, *353*, 84−90.
(11) Veluswamy, H. P.; Kumar, S.; Kumar, R.; Rangsunvigit, P.; Linga, P. Enhanced clathrate hydrate formation kinetics at near ambient temperatures and moderate pressures: Application to natural gas storage. *Fuel* **2016**, *182*, 907−919.
(12) Fleyfel, F.; Devlin, J. P. FT-IR spectra of 90 K films of simple, mixed, and double clathrate hydrates of trimethylene oxide, methyl chloride, carbon dioxide, tetrahydrofuran, and ethylene oxide containing decoupled D_2O. *J. Phys. Chem. B* **1988**, *92*, 631−635.
(13) Ghosh, J.; Methikkalam, R. R. J.; Bhuin, R. G.; Ragupathy, G.; Choudhary, N.; Kumar, R.; Pradeep, T. Clathrate hydrates in interstellar environment. *Proc. Natl. Acad. Sci. U.S.A.* **2019**, *116*, 1526−1531.
(14) Kargel, J. S.; Lunine, J. I. *Solar System Ices*, Based on Reviews Presented at the International Symposium "Solar System Ices" held in Toulouse, France, on March 27−30, 1995; Schmitt, B.; De Bergh, C.; Festou, M., Eds.; Springer: Netherlands: Dordrecht, 1998; pp 97−117.
(15) Fecht, H. J. Defect-induced melting and solid-state amorphization. *Nature* **1992**, *356*, 133−135.
(16) Badan, C.; Heyrich, Y.; Koper, M. T. M.; Juurlink, L. B. F. Surface Structure Dependence in Desorption and Crystallization of Thin Interfacial Water Films on Platinum. *J. Phys. Chem. Lett.* **2016**, *7*, 1682−1685.
(17) Levinger, N. E. Water in Confinement. *Science* **2002**, *298*, 1722−1723.
(18) Ghormley, J. A.; Hochanadel, C. J. Amorphous Ice: Density and Reflectivity. *Science* **1971**, *171*, 62−64.
(19) Stevenson, K. P.; Kimmel, G. A.; Dohnálek, Z.; Smith, R. S.; Kay, B. D. Controlling the Morphology of Amorphous Solid Water. *Science* **1999**, *283*, 1505−1507.
(20) Bar-nun, A.; Herman, G.; Laufer, D.; Rappaport, M. L. Trapping and release of gases by water ice and implications for icy bodies. *Icarus* **1985**, *63*, 317−332.
(21) Thürmer, K.; Nie, S. Formation of hexagonal and cubic ice during low-temperature growth. *Proc. Natl. Acad. Sci. U.S.A.* **2013**, *110*, 11757−11762.
(22) Svishchev, I. M.; Kusalik, P. G. Electrofreezing of Liquid Water: A Microscopic Perspective. *J. Am. Chem. Soc.* **1996**, *118*, 649−654.
(23) Bar-Nun, A.; Dror, J.; Kochavi, E.; Laufer, D. Amorphous water ice and its ability to trap gases. *Phys. Rev. B* **1987**, *35*, 2427−2435.
(24) Bhuin, R. G.; Methikkalam, R. R. J.; Sivaraman, B.; Pradeep, T. Interaction of Acetonitrile with Water-Ice: An Infrared Spectroscopic Study. *J. Phys. Chem. C* **2015**, *119*, 11524−11532.
(25) Herrero, V. J.; Gálvez, Ó.; Maté, B.; Escribano, R. Interaction of CH_4 and H_2O in ice mixtures. *Phys. Chem. Chem. Phys.* **2010**, *12*, 3164−3170.
(26) Ghosh, J.; Hariharan, A. K.; Bhuin, R. G.; Methikkalam, R. R. J.; Pradeep, T. Propane and propane-water interactions: a study at cryogenic temperatures. *Phys. Chem. Chem. Phys.* **2018**, *20*, 1838−1847.
(27) Buch, V.; Devlin, J. P.; Monreal, I. A.; Jagoda-Cwiklik, B.; Uras-Aytemiz, N.; Cwiklik, L. Clathrate hydrates with hydrogen-bonding guests. *Phys. Chem. Chem. Phys.* **2009**, *11*, 10245−10265.
(28) Park, Y.; Shin, S.; Kang, H. Entropy-Driven Spontaneous Reaction in Cryogenic Ice: Dissociation of Fluoroacetic Acids. *J. Phys. Chem. Lett.* **2018**, *9*, 4282−4286.
(29) Blake, D.; Allamandola, L.; Sandford, S.; Hudgins, D.; Freund, F. Clathrate hydrate formation in amorphous cometary ice analogs in vacuo. *Science* **1991**, *254*, 548−551.
(30) Fleyfel, F.; Devlin, J. P. Carbon dioxide clathrate hydrate epitaxial growth: spectroscopic evidence for formation of the simple type-II carbon dioxide hydrate. *J. Phys. Chem. B* **1991**, *95*, 3811−3815.
(31) Richardson, H. H.; Wooldridge, P. J.; Devlin, J. P. FT-IR spectra of vacuum deposited clathrate hydrates of oxirane H_2S, THF, and ethane. *J. Chem. Phys.* **1985**, *83*, 4387−4394.
(32) Kang, S.-P.; Lee, H. Recovery of CO_2 from Flue Gas Using Gas Hydrate: Thermodynamic Verification through Phase Equilibrium Measurements. *Environ. Sci. Technol.* **2000**, *34*, 4397−4400.
(33) Florusse, L. J.; Peters, C. J.; Schoonman, J.; Hester, K. C.; Koh, C. A.; Dec, S. F.; Marsh, K. N.; Sloan, E. D. Stable Low-Pressure Hydrogen Clusters Stored in a Binary Clathrate Hydrate. *Science* **2004**, *306*, 469−471.
(34) Makino, T.; Sugahara, T.; Ohgaki, K. Stability Boundaries of Tetrahydrofuran+Water System. *J. Chem. Eng. Data* **2005**, *50*, 2058−2060.
(35) Lehmkühler, F.; Sakko, A.; Sternemann, C.; Hakala, M.; Nygård, K.; Sahle, C. J.; Galambosi, S.; Steinke, I.; Tiemeyer, S.; Nyrow, A.; et al. Anomalous Energetics in Tetrahydrofuran Clathrate Hydrate Revealed by X-ray Compton Scattering. *J. Phys. Chem. Lett.* **2010**, *1*, 2832−2836.
(36) Hernandez, J.; Uras, N.; Devlin, J. P. Coated Ice Nanocrystals from Water-Adsorbate Vapor Mixtures: Formation of Ether-CO_2 Clathrate Hydrate Nanocrystals at 120 K. *J. Phys. Chem. B* **1998**, *102*, 4526−4535.
(37) Gulluru, D. B.; Devlin, J. P. Rates and Mechanisms of Conversion of Ice Nanocrystals to Ether Clathrate Hydrates: Guest-Molecule Catalytic Effects at ∼120 K. *J. Phys. Chem. A* **2006**, *110*, 1901−1906.
(38) Hallbrucker, A. A clathrate hydrate of nitric oxide. *Angew. Chem., Int. Ed.* **1994**, *33*, 691−693.
(39) Hallbrucker, A.; Mayer, E. Unexpectedly stable clathrate hydrates formed from microporous vapor-deposited amorphous solid water at low "external" guest pressures and their astrophysical implications. *Icarus* **1991**, *90*, 176−180.
(40) Hallbrucker, A.; Mayer, E. Unexpectedly stable nitrogen, oxygen, carbon monoxide and argon clathrate hydrates from vapour-deposited amorphous solid water: an X-ray and two-step differential scanning calorimetry study. *J. Chem. Soc., Faraday Trans.* **1990**, *86*, 3785−3792.
(41) Mayer, E.; Hallbrucker, A. Unexpectedly stable nitrogen and oxygen clathrate hydrates from vapour deposited amorphous solid water. *J. Chem. Soc., Chem. Commun.* **1989**, 749−751.
(42) Hallbrucker, A. Raman spectroscopic monitoring of oxygen clathrate hydrate formation from microporous amorphous solid water. *J. Chem. Soc., Faraday Trans.* **1994**, *90*, 293−295.
(43) Hallbrucker, A.; Mayer, E. Formation and decomposition of oxygen clathrate hydrate as seen by two-step differential scanning calorimetry; novel method for investigating reactions accompanied by gas release. *J. Chem. Soc., Chem. Commun.* **1990**, 873−874.
(44) Duarte, A. R. C.; Shariati, A.; Rovetto, L. J.; Peters, C. J. Water Cavities of sH Clathrate Hydrate Stabilized by Molecular Hydrogen: Phase Equilibrium Measurements. *J. Phys. Chem. B* **2008**, *112*, 1888−1889.
(45) Bag, S.; Bhuin, R. G.; Methikkalam, R. R. J.; Pradeep, T.; Kephart, L.; Walker, J.; Kuchta, K.; Martin, D.; Wei, J. Development of Ultralow Energy (1-10 eV) Ion Scattering Spectrometry Coupled with Reflection Absorption Infrared Spectroscopy and Temperature Programmed Desorption for the Investigation of Molecular Solids. *Rev. Sci. Instrum.* **2014**, *85*, No. 014103.
(46) Moon, E.-S.; Heon, K.; Yasuhiro, O.; Naoki, W.; Akira, K. Direct Evidence for Ammonium Ion Formation in Ice through Ultraviolet-induced Acid-Base Reaction of NH_3 with H_3O^+. *Astrophys. J.* **2010**, *713*, 906−911.
(47) Kim, Y.; Moon, E-s.; Shin, S.; Kang, H. Acidic Water Monolayer on Ruthenium(0001). *Angew. Chem., Int. Ed.* **2012**, *51*, 12806−12809.
(48) Kang, H.; Shin, T. H.; Park, S. C.; Kim, I. K.; Han, S. J. Acidity of Hydrogen Chloride on Ice. *J. Am. Chem. Soc.* **2000**, *122*, 9842−9843.
(49) Monreal, I. A.; Devlin, J. P.; Maşlakcı, Z.; Çiçek, M. B.; Uras-Aytemiz, N. Controlling Nonclassical Content of Clathrate Hydrates

DOI: 10.1021/acs.jpcc.9b04370
J. Phys. Chem. C 2019, 123, 16300−16307

Through the Choice of Molecular Guests and Temperature. *J. Phys. Chem. A* **2011**, *115*, 5822−5832.
(50) Frisch, M. J.; Trucks, G. W.; Schlegel, H. B.; Scuseria, G. E.; Robb, M. A.; Cheeseman, J. R.; Scalmani, G.; Barone, V.; Petersson, G. A.; Nakatsuji, H.; et al. *Gaussian 09*, revision B.01; Gaussian Inc.: Wallingford, CT, 2009.
(51) Jenniskens, P.; Blake, D. F. Structural transitions in amorphous water ice and astrophysical implications. *Science* **1994**, *265*, 753−756.
(52) Monreal, I. A.; Cwiklik, L.; Jagoda-Cwiklik, B.; Devlin, J. P. Classical to Nonclassical Transition of Ether-HCN Clathrate Hydrates at Low Temperature. *J. Phys. Chem. Lett.* **2010**, *1*, 290−294.
(53) Backus, E. H. G.; Grecea, M. L.; Kleyn, A. W.; Bonn, M. Surface Crystallization of Amorphous Solid Water. *Phys. Rev. Lett.* **2004**, *92*, No. 236101.
(54) Wong, A.; Shi, L.; Auchettl, R.; McNaughton, D.; Appadoo, D. R. T.; Robertson, E. G. Heavy snow: IR spectroscopy of isotope mixed crystalline water ice. *Phys. Chem. Chem. Phys.* **2016**, *18*, 4978−4993.
(55) Bergren, M. S.; Schuh, D.; Sceats, M. G.; Rice, S. A. The OH stretching region infrared spectra of low density amorphous solid water and polycrystalline ice Ih. *J. Chem. Phys.* **1978**, *69*, 3477−3482.
(56) Bhuin, R. G.; Methikkalam, R. R. J.; Bag, S.; Pradeep, T. Diffusion and Crystallization of Dichloromethane within the Pores of Amorphous Solid Water. *J. Phys. Chem. C* **2016**, *120*, 13474−13484.
(57) Hill, C. R.; Mitterdorfer, C.; Youngs, T. G. A.; Bowron, D. T.; Fraser, H. J.; Loerting, T. Neutron Scattering Analysis of Water's Glass Transition and Micropore Collapse in Amorphous Solid Water. *Phys. Rev. Lett.* **2016**, *116*, No. 215501.
(58) Mitterdorfer, C.; Bauer, M.; Youngs, T. G. A.; Bowron, D. T.; Hill, C. R.; Fraser, H. J.; Finney, J. L.; Loerting, T. Small-angle neutron scattering study of micropore collapse in amorphous solid water. *Phys. Chem. Chem. Phys.* **2014**, *16*, 16013−16020.
(59) Mitterdorfer, C.; Bauer, M.; Loerting, T. Clathrate hydrate formation after CO_2−H_2O vapour deposition. *Phys. Chem. Chem. Phys.* **2011**, *13*, 19765−19772.
(60) Jenniskens, P.; Blake, D. F. Crystallization of Amorphous Water Ice in the Solar System. *Astrophys. J.* **1996**, *473*, 1104−1113.
(61) Smith, R. S.; Petrik, N. G.; Kimmel, G. A.; Kay, B. D. Thermal and Nonthermal Physiochemical Processes in Nanoscale Films of Amorphous Solid Water. *Acc. Chem. Res.* **2012**, *45*, 33−42.
(62) Hage, W.; Hallbrucker, A.; Mayer, E.; Johari, G. P. Crystallization kinetics of water below 150 K. *J. Chem. Phys.* **1994**, *100*, 2743−2747.
(63) Rao, C. N. R.; Rao, K. J. *Phase Transitions in Solids: An Approach to the Study of the Chemistry and Physics of Solids*; McGraw-Hill: New York, 1978; pp 81−173.
(64) Yuan, C.; Smith, R. S.; Kay, B. D. Communication: Distinguishing between bulk and interface-enhanced crystallization in nanoscale films of amorphous solid water. *J. Chem. Phys.* **2017**, *146*, No. 031102.
(65) Kondo, T.; Kato, H. S.; Bonn, M.; Kawai, M. Deposition and crystallization studies of thin amorphous solid water films on Ru(0001) and on CO-precovered Ru(0001). *J. Chem. Phys.* **2007**, *127*, No. 094703.
(66) Safarik, D. J.; Mullins, C. B. The nucleation rate of crystalline ice in amorphous solid water. *J. Chem. Phys.* **2004**, *121*, 6003−6010.
(67) Smith, R. S.; Matthiesen, J.; Knox, J.; Kay, B. D. Crystallization Kinetics and Excess Free Energy of H_2O and D_2O Nanoscale Films of Amorphous Solid Water. *J. Phys. Chem. A* **2011**, *115*, 5908−5917.
(68) Lee, D. H.; Kang, H. Acid-Promoted Crystallization of Amorphous Solid Water. *J. Phys. Chem. C* **2018**, *122*, 24164−24170.

DOI: 10.1021/acs.jpcc.9b04370
J. Phys. Chem. C 2019, 123, 16300−16307